metals

MDPI

Article

Physical Modelling of Aluminum Refining Process Conducted in Batch Reactor with Rotary Impeller

Mariola Saternus * and Tomasz Merder

Department of Extractive Metallurgy and Environmental Protection, Faculty of Engineering Materials and Metallurgy, Silesian University of Technology, Krasińskiego 8, Katowice 40-019, Poland; Tomasz.Merder@polsl.pl

* Correspondence: Mariola.Saternus@polsl.pl; Tel.: +48-32-603-4275

Received: 13 August 2018; Accepted: 12 September 2018; Published: 15 September 2018

Abstract: The refining process is one of the essential stages of aluminum production. Its main aim is to remove hydrogen, that causes porosity and weakens the mechanical and physical properties of casting aluminum. The process is mainly conducted by purging inert gas through the liquid metal, using rotary impellers. The geometry of the impellers and the processing parameters, such as flow rate of gas and rotary impeller speed, influence the gas dispersion level, and therefore the efficiency of the process. Improving the process, and optimization of parameters, can be done by physical modelling. In this paper, the research was carried out with the use of a water model of batch reactor, testing three different rotary impellers. Varied methods were used: visualization, which can help to evaluate the level of dispersion of gas bubbles in liquid metal; determination of residence time distribution (RTD) curves, which was obtained by measuring the conductivity of NaCl tracer in the fluid; and indirect studies, completed by measuring the content of dissolved oxygen in water to simulate hydrogen desorption. The research was carried out for different processing parameters, such as flow rate of refining gas (5–25 $L \cdot min^{-1}$) and rotary impeller speed (3.33–8.33 s^{-1}). The obtained results were presented graphically and discussed in detail.

Keywords: aluminum; refining; physical modelling; RTD curves

1. Introduction

Undoubtedly, hydrogen is one of the most harmful impurities in liquid aluminum, and its alloys, due to porosity, which in turn deteriorates the physical and mechanical properties of aluminum castings [1–3]. Currently, the refining process is becoming one of the most important steps in the production of primary and secondary aluminum. Although there are various methods used for the refining process (e.g., chlorine or non-chlorine route, powder injection or purging by gas, stirring by rotary impeller, and filtering by ceramic foam filters), the process of blowing the melt with refining gas, mainly argon, seems to be the most popular [4–6]. Its main purpose is to remove hydrogen from liquid metal, but flotation also enables the elimination of up to 90% of nonmetallic impurities [5,6]. This method of gas injection can be carried out with the use of porous plugs, lances, diffusers, rotating nozzles and rotary impellers, the latter of which is widely used in aluminum foundries worldwide because of promising results [7–9]. The idea of this method of refining, is to inject gas bubbles through the rotary impeller shaft, which, as a result of rotor agitation, can be appropriately small. The mixing of the small gas bubbles with the liquid metal depend on the geometry of the rotary impeller [10]. The gas bubble circulation and dispersion, in the aluminum, is one of the most important factors in obtaining a large gas liquid contact area. Oldshue et al. [11] proposed four different patterns of gas liquid mixture: (a) flooding or channeling, (b) minimum dispersion, (c) intimate dispersion and (d) uniform dispersion. The last two cases are promoted most, in order to achieve a good level of hydrogen removal. The flow

pattern of gas bubble dispersion has been investigated by many researchers: Hsi et al. [12] studied the sound spectra in a stirred tank using a hydrophone; Warmoeskerken and Smith [13] determined gas dispersion, based on the gassed power measurement and observation of cavity formation, in a tank with a disc-turbine; Chen and Zhao [14] analyzed dispersion flow patterns, considering the ratio of radial force to the buoyancy force, which prevail close to impeller; Chen and Zhao [15] measured the local pressure fluctuations at points within the gas-liquid mixture; and Chen et al. [16] developed a non-intrusive method, based on characteristic parameters obtained from the pressure fluctuations measured on the gas supply line. To sum up, the dispersion flow patterns strongly depend on the geometry of the rotor impeller and the processing parameters, such as rotary impeller speed and flow rate of refining gas.

To determine the impact of the above mentioned parameters on the level of gas dispersion, physical modelling is applied. This method gives good results because of the use of water as a modeling medium due to availability, low cost, transparency of the model tank and simplicity in model buildings after meeting geometric, dynamic and kinematic similarities [17,18]. The fulfilment of such similarities, according to the theory of dimension analysis, are realized based on the equality of the relevant criterial numbers in the model with the object under study. When designing a physical model of the refining process, conducted in a refining reactor with rotary impellers, the most important numbers are: Euler, Reynolds, Froude and Weber [18]. Several physical water models have been built, and many researchers [19–22] have investigated various factors such as: Design of rotary impellers [23], gas bubbles ascending velocity [24], vortex formation [25], gas removal kinetics [26], dispersion levels and the removal of dissolved oxygen from water by refining gases [1,22], and CO_2 adsorption [27]. Models can be either reduced scale or full scale; however, there are certain advantages when using a full-scale model over a reduced scale model [28]. The results of physical modelling can be mainly divided into: visualization methods, such as level of gas dispersion in the liquids; measuring techniques, such as the determination of residence time distribution (RTD), by measuring the conductivity of aqueous solution of some salts (e.g., NaCl); or indirect studies, mainly oxygen desorption techniques in water, simulating hydrogen desorption [29]. RTD curves can be obtained experimentally from the impulse concentration response. The concentrated tracer stream is injected into the liquid metal at a specified time (reference time), and the concentration of tracer in the outlet stream is obtained [30,31] by measuring the conductivity of the fluid. The RTD curve is the concentration of the tracer on the tank output as a function of time, and provides important information about the behavior of the flow gas. It is mainly used in the steel industry to determine the range of transient zones, and to estimate the share of various types of flow, e.g., in ladles or tundishes [28,32–34]. It is also possible to apply particle image velocimetry (PIV) technique to obtain flow fields, and to perform velocity maps and turbulent structure [3,10,21,27,35], or measure the torque of the shaft to determine the mechanical energy supplied into the ladle [27].

The main goals of this study are to obtain complete information about the blowing process of aluminum by argon, using the three mentioned methods (study fluid flow patterns by visualization method, evaluating time of mixing by determining RTD curves, and measuring the content of dissolved oxygen in water continuously and instantaneously), and evaluate the flow behavior for the new rotary impeller. RTD analysis is popularly used in the steel industry, so this study should also answer if this method could be successfully applied in the researching field of rotary impeller degassing process.

2. Materials and Methods

The system under study is presented schematically in Figure 1a, and its dimensions and characteristics are shown in Table 1 and Figure 1b. The test stand consists of a water tank (Figure 1c) made of Plexiglas, simulating the URO-200 batch refining model (IMN, Skawina, Poland), control panel, impeller driver, and measuring apparatus for determining RTD curves. Figure 1b also presents placement of three conductometers, for measuring the conductivity of the aqueous NaCl solution, and the location of two sensors, for measuring oxygen desorption from water. The physical model was

built on a 1:1 scale, according to the theory of similarity. If the results obtained from physical modeling can be representative, and could be transferred to real conditions, physical models are built according to strictly defined principles resulting from the theory of similarity. The similarity of physical models of reactors for aluminum refining requires the preservation of similarity criteria, both geometric and dynamic, for water and aluminum. In these models, this is accomplished by means of appropriate criterial numbers. The assumption that the flow in the refining reactor is isothermal and laminar enables the criterial equation to be written in the following form:

$$\varphi(Eu,\ Sl,\ Fr,\ Re) = 0 \tag{1}$$

where *Eu*—Euler's number, *Sl*—Strouhal's number, *Fr*—Froude's number and *Re*—Reynold's number.

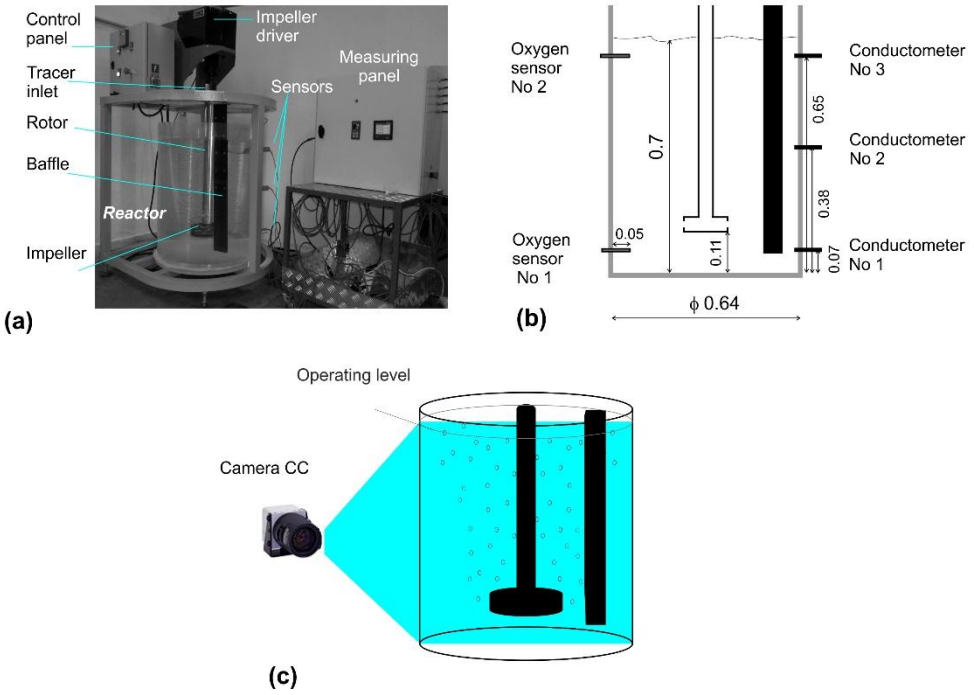

Figure 1. Physical modelling test stand: (**a**) View of the test stand with all elements; (**b**) a scheme of the refining model, with marked places of conductometers and fixed oxygen sensors, and the most important dimensions (in m) of the model; (**c**) the idea of measuring refining gas dispersion in the model reactor.

Strouhal's (*Sl)* criterion can be excluded because the character of the liquid flow is close to laminar. Euler's (*Eu*) criterion, which has significance in flows under pressure, can be neglected in cases of flow in open reactors. In the studied system, the flow is steady and the Reynold's number (*Re*) is in the range of self-modelling. Laminar flows are characterized by small Reynold's numbers, whereas turbulent flows are characterized by high Reynold's numbers, and often transfer from laminar motion to turbulent motion is rapid, and the limiting values of the *Re* number are then defined as critical. In this range of flows, the values of the *Re* number are changing insignificantly. Thus, there is no necessity in this area to obtain the equality of criterial numbers. Therefore, the dominating criterion determining the similarity of studied model to real object is Froude's (*Fr*) criterion. Equation (1) can be then written in the following form:

$$\varphi(Fr) = 0 \tag{2}$$

Additionally, the Weber's number, which characterizes the influence of surface tension on the flow of liquid, is the criterion number supporting the achievement of the required similarity of the

model to the real object. Table 1 shows the values of calculated criterial numbers (Reynolds, Froude and Weber) for water, at a temperature of 293 K, and aluminum, at a temperature of 973 K.

A well-constructed model gives results that are approximate to those obtained in real conditions, and the criterion numbers are used to preserve the similarity of the model to the real object without physically affecting the process itself—they describe it, but do not direct it.

Table 1. Main characteristics and dimensions of URO-200 water model and comparison of criterial numbers for water and aluminum, calculated for URO-200 reactor for rotary impeller speed 5.00 s^{-1}.

Characteristic Feature				**Value**		
Volume of the Tank				230 L		
Velocity of Gas Bubble Flow (rotary impeller speed x distance from rotary impeller axis)			Impeller A 0.375 m·s^{-1}	Impeller B 0.475 m·s^{-1}		Impeller C 0.350 m·s^{-1}
Rotary Impeller Diameter			Impeller A 0.15 m	Impeller B 0.19 m		Impeller C 0.14 m
Criterial Numbers						
Fluid		water		aluminum		
Temperature		293 K		973 K		
Dynamic Viscosity		1005 Pa·s		1000 Pa·s		
Surface Tension		0.072 N·m^{-1}		0.868 N·m^{-1}		
Density		1000 kg·m^{-3}		2700 kg·m^{-3}		
Reynold's Number	Impeller A 56,250	Impeller B 90,250	Impeller C 49,000	Impeller A 151,875	Impeller B 243,675	Impeller C 132,300
Weber's Number	292.97	595.40	238.19	65.61	133.35	53.35
Froude's Number	0.095	0.121	0.089	0.095	0.121	0.089

The modelling research was conducted for three different rotary impellers—one of them was a new design, and two were commercial designs (see Figure 2). The research was carried out in the range of processing parameters: rotary impeller from 3.33 to 8.33 s^{-1}, and flow rate of refining gas from 5 to 25 L·min^{-1}. However, based on earlier research [1,9,29,36], and their primary results, the number of measurements were decreased to 27, and according to Table 2, the extreme values of flow rate were skipped.

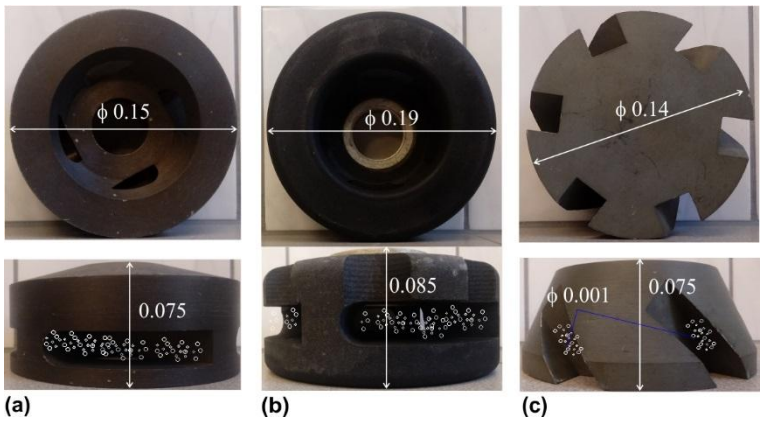

Figure 2. View of the rotary impellers applied in the measurements: (**a**) commercial impeller design A; (**b**) new impeller design B; (**c**) commercial impeller design C. Unit: m.

The research methodology was as follows:

- The model tank was filled with water up to 0.7 m, and the processing parameters were changed according to Table 2.
- Visualization research was carried out by digital camera, recording the dispersion level for all rotary impellers, whilst changing the processing parameters.

- Next, the tank was saturated with oxygen. The saturation level was measured by two oxygen meters CO-401, Elmetron, Zabrze, Poland (location of oxygen meters is shown in Figure 1b). After reaching the saturation level, argon was introduced into the model by rotary impeller, and processing parameters were according to the variants in Table 2. Removal of oxygen from water, as an analog of hydrogen removal from aluminum [1,22,27], was measured every 0.5 min. The process of aluminum refining in the batch reactor typically lasted 10 min, therefore the process of oxygen removal was carried out for every variant for 10 min.
- Finally, for the selected variants, based on visualization results (dispersion level), RTD curves were measured, the NaCl tracer was poured from the top of the tank with water, the measuring device was switched on, and the three conductometers measured the change in conductivity at three different locations of the reactor model. The obtained results were automatically registered by the computer system.

Table 2. Experimental variables for water physical modelling.

Rotary Impeller A								
No.	**Impeller Speed, s^{-1}**	**Gas Flow Rate, L·min^{-1}**	**No.**	**Impeller Speed, s^{-1}**	**Gas Flow Rate, L·min^{-1}**	**No.**	**Impeller Speed, s^{-1}**	**Gas Flow Rate, L·min^{-1}**
P1	5.00 (300 rpm)	10	P2	6.66 (400 rpm)	10	P3	8.33 (500 rpm)	10
P4		15	P5		15	P6		15
P7		20	P8		20	P9		20
Rotary Impeller B								
No.	**Impeller Speed, s^{-1}**	**Gas Flow Rate, L·min^{-1}**	**No.**	**Impeller Speed, s^{-1}**	**Gas Flow Rate, L·min^{-1}**	**No.**	**Impeller Speed, s^{-1}**	**Gas Flow Rate, L·min^{-1}**
S1	5.00	10	S2	6.66	10	S3	8.33	10
S4		15	S5		15	S6		15
S7		20	S8		20	S9		20
Rotary Impeller C								
No.	**Impeller Speed, s^{-1}**	**Gas Flow Rate, L·min^{-1}**	**No.**	**Impeller Speed, s^{-1}**	**Gas Flow Rate, L·min^{-1}**	**No.**	**Impeller Speed, s^{-1}**	**Gas Flow Rate, L·min^{-1}**
R1	5.00	10	R2	6.66	10	R3	8.33	10
R4		15	R5		15	R6		15
R7		20	R8		20	R9		20

3. Results and Discussions

3.1. Visualisation Results

The results of the visualization measurements are presented in Figure 3 for impeller A, Figure 4 for impeller B, and Figure 5 for impeller C. These pictures show the level of dispersion for various processing parameters. As mentioned earlier, the results were unsatisfactory under the extreme conditions of 5 and 25 L·min^{-1}, and 3.33 s^{-1}. For 5 L·min^{-1} and 3.33 s^{-1}, in all cases, the flooding pattern of dispersion (gas rises axially as a bubble column) was observed for all rotary impellers. The flooding pattern, or minimum dispersion, was seen when the flow rate of refining gas was 5 L·min^{-1} and with the remaining rotary impeller speeds (5.00, 6.66 and 8.33 s^{-1}). Thus, this variant was omitted in further studies. Similar patterns were observed for 3.33 s^{-1} and flow rates of gas from 10 to 25 L·min^{-1}. Consequently, these variants were also omitted in further studies. For the flow rate of 25 L·min^{-1}, the uniform dispersion was observed at all rotary impeller speeds, but swirls were also created, and gas bubbles formed chains that caused waves on the surface. This is dangerous, especially under industrial conditions, because the hydrogen could be reintroduced into the liquid metal. Therefore, this case was also rejected.

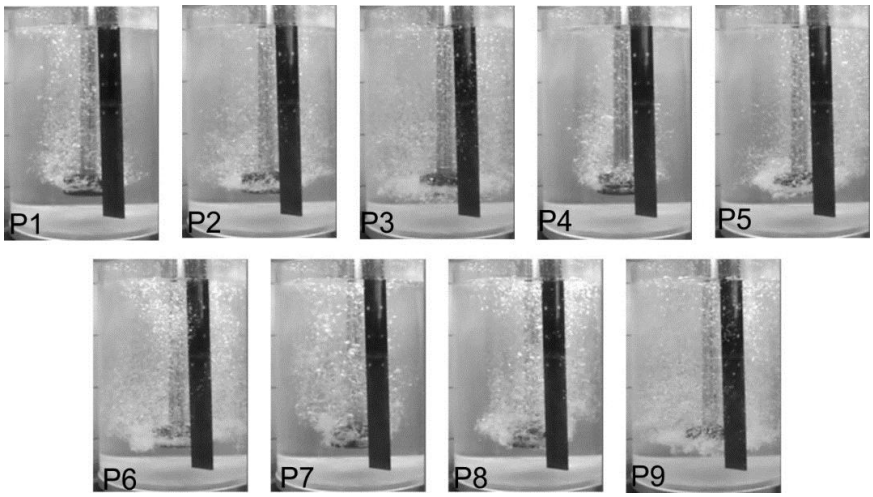

Figure 3. The level of dispersion registered for different processing parameters, according to Table 2, for the commercial design rotary impeller A.

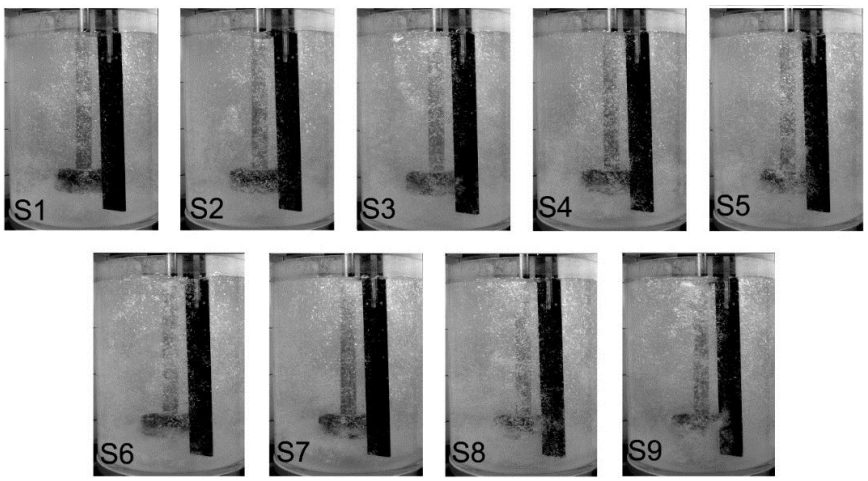

Figure 4. The level of dispersion registered for different processing parameters, according to Table 2, for the new design rotary impeller B.

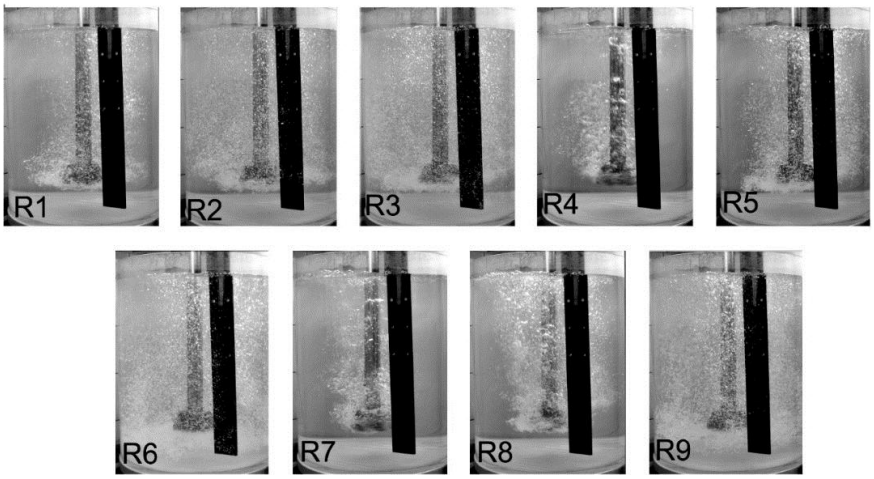

Figure 5. The level of dispersion registered for different processing parameters, according to Table 2, for the commercial design rotary impeller C.

For impeller A, a minimum dispersion level was observed when the rotary impeller speed was 5.00 s^{-1} and the flow rate of the refining gas was 10, 15 and 20 $L \cdot min^{-1}$ (variants P1, P4 and P7), as well as for 6.66 s^{-1} and 10 and 15 $L \cdot min^{-1}$ (variants P2 and P7). This means that single gas bubbles were rising to the top of the reactor, and the mixing of gas bubbles is near the shaft of the rotary impeller. The best results (uniform dispersion) were obtained with the rotary impeller speed of 8.33 s^{-1} for almost all refining gas flow rate values (variants P3, P6 and P9).

For impeller B, in all cases, intimate or uniform dispersion were noticed. For variants S1, S4 and S7 the intimate dispersion was seen. The best results were obtained for variants S3 and S6, with a rotary impeller speed of 8.33 s^{-1} and flow rates of refining gas of 10 and 15 $L \cdot min^{-1}$. In case of variant S9, excessive dispersion was seen—chains of gas bubbles were created causing swirls.

For impeller C, variants R1, R4 and R7 produced the worst results (5 s^{-1} and 10, 15, 20 $L \cdot min^{-1}$) i.e., minimum dispersion was observed. The uniform dispersion could be seen when the rotary impeller speed was 8.33 s^{-1} and the flow rates of refining gas were 10 and 15 $L \cdot min^{-1}$. In these variants (R6 and R9), the single gas bubbles are rising to the top of the reactor, gas bubbles are uniformly mixed with water in the whole model of refining reactor, even beneath the rotary impeller, and the mixing of gas bubbles with water exists. Figure 6 shows the exemplary variants with different cases of dispersion levels: (a) minimum dispersion—single gas bubbles rise to the top of the reactor, dispersion is observed only in the area of gas bubble generation, and lack of dispersion in the whole volume of the tank, (b) excessive dispersion—creation of bubble chains and swirls, (c) uniform dispersion—good mixing of gas bubbles with liquid is observed in the whole volume of the tank. Table 3 summarizes the results of visualization, showing types of dispersion for all studied impellers.

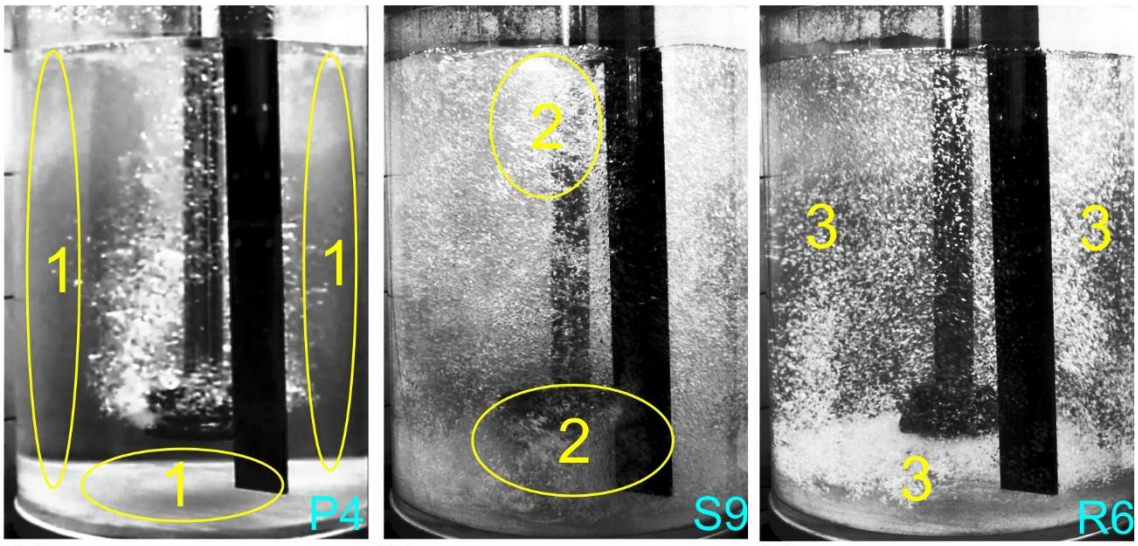

Figure 6. The exemplary variants of dispersion level with marked places indicating dead zones without mixing (1), swirls and chains of bubbles (2), and areas of uniform mixing of gas bubbles with water (3): (**a**) minimal dispersion, (**b**) excessive dispersion, (**c**) uniform dispersion.

Table 3. Summary of visualization results—different types of gas bubble dispersion in water, for flow rate of refining gas in range: 10–20 L·min^{-1}, and rotary impeller speed: 5.00–8.33 s^{-1}, for three studied rotary impellers.

Flow Rate of Refining Gas, L·min^{-1}	Type of Dispersion		
	Rotary Impeller Speed, s^{-1}		
	5.00	6.66	8.33
Impeller A			
10	Minimum	Minimum	Uniform
15	Minimum	Minimum	Uniform
20	Minimum	Intimate	Uniform
Impeller B			
10	Intimate	Uniform	Uniform
15	Intimate	Uniform	Uniform
20	Intimate	Uniform	Excessive uniform
Impeller C			
10	Minimum	Intimate	Uniform
15	Minimum	Intimate	Uniform
20	Minimum	Intimate	Uniform

3.2. The Research of Oxygen Removal from Water

The research of oxygen removal from water was carried out for all variants presented in Table 2. The level of oxygen concentration was measured in two places (see Figure 1b); however, the results were similar (the placement of sensors was investigated by Chin et al. [37], which indicated that curves for the sensor located in the lower and upper part of the reactor are almost identical). Therefore, the results of the research presented graphically in Figure 7 show the measurements of the top oxygen meter only. In all cases the best results of removing oxygen were obtained for rotary impeller B, they were considerably better than for impeller A and C. The results of impellers A and C were comparable, though rotary impeller C was insignificantly better. In case of flow rate of refining gas 10 L·min^{-1}, the rotary impeller speed played a significant role in obtaining a better level of oxygen removal. For impeller A and C, at 5.00 s^{-1} about 10 mg·L^{-1} oxygen content was obtained, whereas at 8.33 s^{-1} this level was lower, reaching about 5 mg·L^{-1}. In case of rotary impeller B, at 5.00 s^{-1} the oxygen content was 3 mg·L^{-1}. The same oxygen level was obtained much faster for the rotary impeller speed 8.33 s^{-1} (about 400 s).

For the flow rate of refining gas 15 L·min^{-1} at 5.00 s^{-1}, the oxygen concentration for impeller A was 9 mg·L^{-1}, and for impeller C 8 mg·L^{-1}, whereas for impeller B only 2 mg·L^{-1}. Better results were obtained for rotary impeller speeds 6.6 s^{-1} and 8.33 s^{-1}—for impeller A: 6 and 4 mg·L^{-1}, and for impeller C: 5 and 2.5 mg·L^{-1}, respectively. For impeller B, the levels of oxygen concentration 2 mg·L^{-1} were reached after 500 s at 6.66 s^{-1} and after 400 s at 8.33 s^{-1}.

For the case of flow rate of refining gas 20 L·min^{-1}, the results of oxygen concentration for 5.00 s^{-1} were comparable with those for 15 L·min^{-1}. This was similar for 6.66 and 8.33 s^{-1} rotary impeller speeds. However, for rotary impeller B, the time taken to obtain level of oxygen concentration 2 mg·L^{-1} for rotary impeller speed 8.33 s^{-1} was quicker, and reached 300 s.

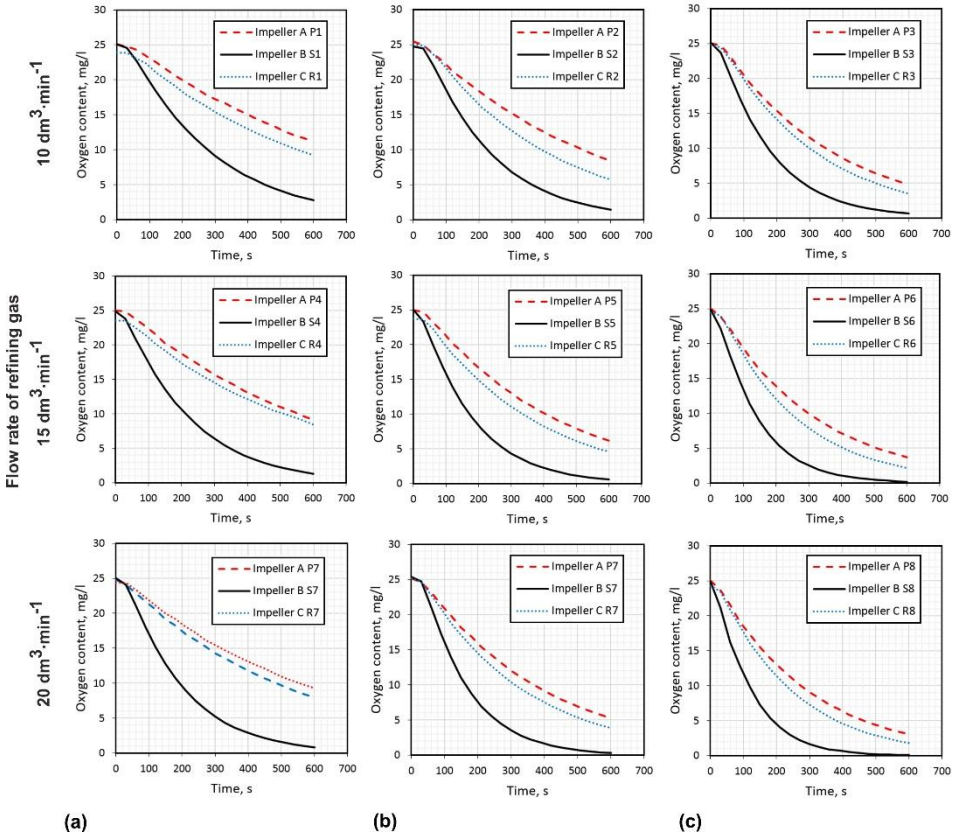

Figure 7. Results of research concerning oxygen removal from water model of batch reactor for aluminum refining, by argon blowing, for three different impellers. Flow rate of refining gas ranging from 10 to 20 $dm^3 \cdot min^{-1}$ and: (**a**) rotary impeller speed 5.00 s^{-1}; (**b**) rotary impeller speed 6.66 s^{-1}; (**c**) rotary impeller speed 8.33 s^{-1}.

Because the gas consumption is seen as the important operational cost in cast foundries, it is possible to calculate the efficiency of gas consumption (E), which is defined as total volume of purge gas (Vg) needed to eliminate 90% of the dissolved oxygen, and can be written in the following form [27]:

$$E = \frac{([O_2]_o - [O_2]_{0.1})}{Vg} \quad (3)$$

Table 4 shows the results of efficiency of gas consumption for the three studied rotary impellers, and Table 5 presents the total time to eliminate 90% of dissolved oxygen. The best gas consumption was achieved for the new design rotary impeller. For this impeller, the total time needed to eliminate 90% of dissolved oxygen for all variants was smaller than 630 s.

Table 4. Efficiency of gas consumption for studied rotary impellers, for variants P8, S7 and R7.

Type of Rotary Impeller	Variant	Efficiency of Gas Consumption E, ppm/liter
Rotary impeller A	P8	0.045
Rotary impeller B	S7	0.065
Rotary impeller C	R7	0.054

Table 5. Total time needed to eliminate 90% of dissolved oxygen for chosen variants of rotary impellers.

Rotary Impeller A		Rotary Impeller B		Rotary Impeller C	
Variants	Time, s	Variants	Time, s	Variants	Time, s
P1	1200	S1	630	R1	1020
P2	1020	S2	510	R2	780
P3	810	S3	390	R3	660
P4	1050	S4	480	R4	930
P5	870	S5	390	R5	720
P6	720	S6	300	R6	570
P7	930	S7	420	R7	1050
P8	750	S8	360	R8	690
P9	660	S9	270	R9	540

3.3. Determination of Residence Time Distribution(RTD) Curves

Theoretical basis of RTD characteristics has the source in the inert function of age distribution, which assumes that in the period between t and Δt the fraction of substance being in reactor equals the product of $I(t)\cdot\Delta t$, $I(t)$. It is a continuous function and after arrangement the relationship can be written in the following form:

$$\int_0^\infty I(t)dt = 1 \tag{4}$$

When assuming the reactor is in equilibrium state, the transport of fluid at the inlet and outlet have advective character and liquid is incompressible, such function can be written in the form:

$$\int_0^\infty E(t)dt = 1 \tag{5}$$

where $E(t)$ can be defined as:

$$E(t) = \frac{C(t)}{\int_0^\infty C(t)dt} \tag{6}$$

where $C(t)$ change of tracer in liquid metal or water as a function of time.

Determination of RTD curves based on measurement of conductivity changes in water with added tracer (aqueous NaCl solution) is in $\mu S\cdot cm^{-1}$. If the obtained results were comparable, the recorded values are calculated to a dimensionless form according to the following Equations (7) and (8) [37]:

$$C = \frac{G_{pom}}{G_{max}} \tag{7}$$

$$C_b = \frac{c - c_o}{c_\infty - c_o} \tag{8}$$

where C—basic dimensionless tracer concentration, G_{pom}—analog of tracer concentration in time, $\mu S\cdot cm^{-1}$, G_{max}—analog of maximal tracer concentration in modelling liquid, $\mu S\cdot cm^{-1}$, C_b—dimensionless concentration of the tracer, c_o—base dimensionless concentration of the tracer at the beginning of the process, c_∞—base dimensionless concentration of the tracer at the end of the process.

The determined characteristics make it possible to determine the minimum mixing times of the tracer in the modelling fluid (water). The criterion, which should be fulfilled to determine such values, is the moment when the concentration of the marker for both measuring points reached a plateau in the range of 0.9–1.1, this meant that the tracer was completely mixed into the entire volume of the modelling liquid. The RTD curves were measured for chosen processing parameters, including the best and worst visualization results for:

- Impeller A: the worst result (minimum dispersion)—Variant P4 and the best ones P3 and P9.
- Impeller B: the worst result (excessive dispersion)—Variant S9 and the best ones S1 and S6.

- Impeller C: the worst result (minimum dispersion)—Variant R7 and the best ones R6 and R9.

RTD curves for all mentioned above variants were presented in Figure 8 in the form of dimensionless concentration as a function of time. Based on these curves, the shortest time for mixing gas bubbles in the whole reactor were calculated and are summarized in Table 6.

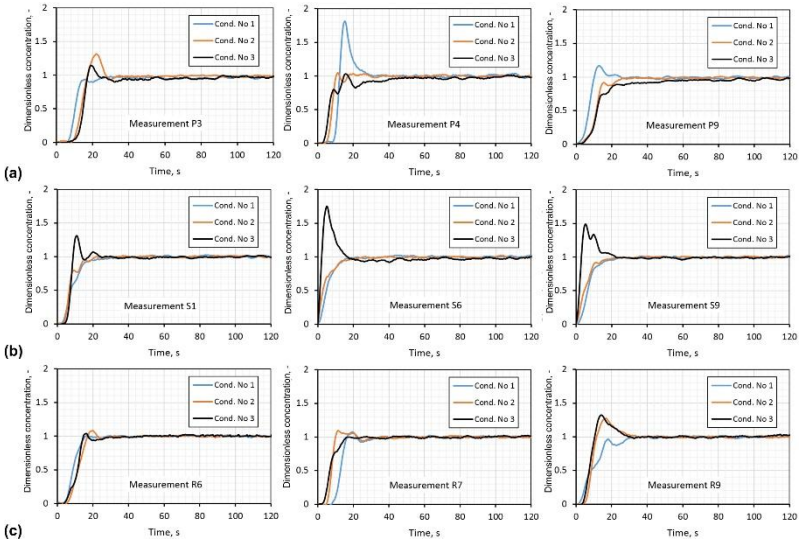

Figure 8. Results of residence time distribution (RTD) curves determination on water model of batch reactor for aluminum refining, by argon blowing, for three different impellers, for chosen processing parameters based on visualization results: (**a**) rotary impeller A; (**b**) rotary impeller B; (**c**) rotary impeller C.

Table 6. Time of mixing gas bubbles with water estimated on the base of RTD curves.

Rotary Impeller A		**Rotary Impeller B**		**Rotary Impeller C**	
Variants	Time, s	Variants	Time, s	Variants	Time, s
P1	32	S1	23	R1	35
P2	35	S2	25	R2	33
P3	30	S3	28	R3	25
P4	45	S4	35	R4	32
P5	40	S5	25	R5	25
P6	32	S6	18	R6	23
P7	31	S7	30	R7	30
P8	30	S8	24	R8	25
P9	30	S9	23	R9	30

Estimated time of mixing is the longest for rotary impeller A variant P4 (5.00 s^{-1}, 15 $L \cdot min^{-1}$), for the last two variants it is shorter (30 s). However, compared with the other two impellers, it was not satisfactory. Results for rotary impeller C were better than that for rotary impeller A, with the shorter time of mixing of 23 s, at rotary impeller speed 8.33 s^{-1} and flow rate of refining gas at 15 $L \cdot min^{-1}$. The best results of mixing time were reached for impeller B, which was 18 s, at a rotary impeller speed of 8.33 s^{-1} and the flow rate of refining gas at 15 $L \cdot min^{-1}$.

4. Conclusions

On the basis of the conducted research, the following conclusions can be drawn:

- Physical modelling is a helpful method for working out the new design rotary impeller and aids easy identification of the optimal processing parameters.

- The physical model of the refining reactor simulates the conditions prevailing in this reactor during refining process. The rates of gas bubble dispersion significantly influences the efficiency of the hydrogen removal process. Determining the optimal range of gas flow increases the efficiency of the purging process, which in turn reduces its costs.
- The information obtained from the dispersion patterns are dependent on observation and interpretation, and thus improper conclusions can be drawn.
- RTD curves, which are quantitative analysis, provide the information about mixing time of tracer with water, and based on such results the identification of processing parameters, such as flow rate of refining gas and rotary impeller speed, is possible. RTD curves do not give a direct and clear answer, but allow for a satisfactory estimation of the technological parameters and the operation of the reactor.
- Based on research of oxygen removal from water, as an analog of hydrogen desorption from aluminum, the essential information can be obtained about the process and processing parameters, and also about the time of refining.
- The new design impeller B had the best results in all applied methods, the best variants being 8.33 s^{-1} and 15 $L \cdot min^{-1}$. The next step of the research should now be to test the new design impeller under industrial conditions.

For better understanding of the process, and to complete the obtained results for the new rotary impeller, the numerical modelling could be applied.

Author Contributions: Conceptualization—M.S. and T.M., methodology—M.S. and T.M., experimental research—M.S., graphical results—T.M., writing and original draft preparation—M.S.

Funding: This research was funded by Polish Ministry for Science and Higher Education under internal grant BK-221/RM0/2018 for Department of Extractive Metallurgy and Environmental Protection, Silesian University of Technology, Poland.

Conflicts of Interest: The authors declare no conflict of interest.

References

1. Saternus, M.; Botor, J. Physical model of aluminium refining process in URC-7000. *Metalurgija* **2009**, *48*, 175–179.
2. Simensen, C.J.; Berg, G. A survey of inclusions in aluminium. *Aluminium* **1980**, *56*, 335–340.
3. Gomez, E.R.; Zenit, R.; Rivera, C.G.; Trapaga, G.; Ramirez-Argaez, M.A. Physical modelling of the fluid flow in ladles of aluminium equipped with impeller and gas purging for degassing. *Metall. Mater. Trans. B* **2013**, *44*, 974–983. [CrossRef]
4. Zhang, L.; Lv, X.; Torgerson, A.T.; Long, M. Removal of impurity elements from molten aluminum: A review. *Miner. Process. Extr. Metll. Rev.* **2011**, *32*, 150–228. [CrossRef]
5. Taylor, M.B. Molten metal fluxing/treatment: How best achieve the desired quality requirements. *Aluminium* **2003**, *79*, 44–50.
6. Waite, P. A Technical perspective on molten aluminum processing. In *Light Metals, the Minerals, Metals and Materials Society*; TMS: Seattle, DC, USA, 2002; pp. 841–848.
7. Camacho-Martinez, J.L.; Ramirez-Argaez, M.A.; Juarez-Hernandez, A.; Gonzalez-Rivera, C.; Trapaga-Martinez, G. Novel degasification design for aluminum using an impeller degasification water physical model. *Mater. Manuf. Process.* **2012**, *27*, 556–560. [CrossRef]
8. Li, J.H.; Hao, Q.T. Develop the degassing and purification equipment of molten aluminum alloys by rotary impeller. *Foundry* **2007**, *56*, 731–734.
9. Saternus, M.; Botor, J. Refining process of aluminium conducted in continuous reactor—Physical model. *Arch. Metall. Mater.* **2010**, *55*, 465–475.
10. Mancilla, E.; Cruz-Mendez, W.; Garduno, I.E.; Gonzalez-Rivera, C.; Ramirez-Argaez, M.A.; Ascanio, G. Comparison of the hydrodynamic performance of rotor-injector devices in a water physical model of an aluminum degassing ladle. *Chem. Eng. Res. Des.* **2017**, *118*, 158–169. [CrossRef]

11. Oldshue, J.Y. *Fluid Mixing Technology*; Chemical Engineering McGraw-Hill Pub. Co.: New York, NY, USA, 1983; pp. 141–154.
12. Hsi, R.; Tay, M.; Bukur, D.; Tatterson, G.; Morrison, G. Sound spectra of gas dispersion in an aerated agitated tank. *Chem. Eng. J.* **1985**, *31*, 153–161. [CrossRef]
13. Warmoeskerken, M.M.C.G.; Smith, J.M. Flooding of disco turbines in gas-liquid dispersion: A new description of the phenomena. *Chem. Eng. Sci.* **1985**, *40*, 2063–2071. [CrossRef]
14. Chen, J.J.J.; Zhao, J.C. Bubble distribution in a melt treatment water model. In *Light Metals, the Minerals, Metals and Materials Society*; TMS: Las Vegas, NV, USA, 1995; pp. 1227–1231.
15. Zhao, J.C.; Chen, J.J.J. Gas line pressure fluctuation analysis of a gas-liquid reactor. *J. Therm Sci.* **2005**, *14*, 267–271.
16. Chen, J.J.J.; Zhao, J.C.; Lacey, P.V.; Gray, T.N.H. Flow pattern in a melt treatment water model based on shaft power measurements. In *Light Metals, the Minerals, Metals and Materials Society*; TMS: New Orleans, LA, USA, 2001; pp. 1021–1025.
17. Odenthal, H.J.; Bölling, R.; Pfeifer, H. Numerical and physical simulation of tundish fluid flow phenomena. *Steel Res.* **2003**, *74*, 44–55. [CrossRef]
18. Saternus, M. *Rafinacja Aluminium I Jego Stopów Przez Przedmuchiwanie Argonem*; Politechnika Śląska: Gliwice, Poland, 2011; pp. 82–87.
19. Evans, J.W.; Field, A.; Mittal, N. Measurements of bubble dispersion and other bubble parameters in a gas fluxing unit at Alcoa using a capacitance probe. In *Light Metals, the Minerals, Metals and Materials Society*; TMS: San Diego, CA, USA, 2003; pp. 909–913.
20. Waz, E.; Carre, J.; Le Brun, P.; Jardy, A.; Xuereb, C.; Ablitzer, D. Physical modelling of the aluminum degassing process: Experimental and mathematical approaches. In *Light Metals, the Minerals, Metals and Materials Society*; TMS: San Diego, CA, USA, 2003; pp. 901–907.
21. Camacho-Martinez, J.L.; Ramirez-Argaez, M.A.; Zenit-Camacho, R.; Juarez-Hernandez, A.; Barceinas-Sanchez, J.O.; Trapaga-Martinez, G. Physical modelling of an aluminum degassing operation with rotating impellers—A comparative hydrodynamic analysis. *Mater. Manuf. Process.* **2010**, *25*, 581–591. [CrossRef]
22. Guofa, M.; Shouping, Q.; Xiangyu, L.; Jitai, N. Research on water simulation experiment of the rotating impeller degassing process. *Mater. Sci. Eng. A* **2009**, *499*, 195–199.
23. Nilmani, M.; Thay, P.; Siemensen, C. A comparative study of impeller performance. In *Light Metals, the Minerals, Metals and Materials Society*; TMS: San Diego, CA, USA, 1992; pp. 939–946.
24. Ohno, Y.; Hampton, D.T.; Moores, A.W. The GBF rotary system for total aluminum refining. In *Light Metals, the Minerals, Metals and Materials Society*; TMS: Denver, CA, USA, 1993; pp. 915–921.
25. Nilmani, M.; Thay, P.K.; Simansen, C.J.; Irwin, D.W. Gas fluxing operation in aluminum melt refining laboratory and plant investigation. In *Light Metals, the Minerals, Metals and Materials Society*; TMS: Anaheim, CA, USA, 1990; pp. 747–754.
26. Johansen, S.; Graadahl, S.; Tetlie, P.; Rasch, B.; Myrbostad, E. Can rotor based refining units be developed and optimized based on water model experiments? In *Light Metals, the Minerals, Metals and Materials Society*; TMS: San Antonio, TX, USA, 1998; pp. 805–810.
27. Hernandez-Hernandez, M.; Camacho-Martinez, J.L.; Gonzalez-Rivera, C.; Ramirez-Argaez, M.A. Impeller design assisted by physical modelling and pilot plant trials. *J. Mater. Process. Technol.* **2016**, *236*, 1–8. [CrossRef]
28. Chattopadhyay, K.; Isac, M.; Guthrie, R.I.L. Physcial and mathematical modelling of steelmaking tundish operations: A review of the last decade (1999–2009). *ISIJ Int.* **2010**, *50*, 331–348. [CrossRef]
29. Saternus, M. Modelling research of hydrogen desorption from liquid aluminum and its alloys. *Metalurgija* **2011**, *50*, 257–260.
30. Wen, C.Y.; Fan, L.T. *Models for Flow Systems and Chemical Reactors*; Chemical Processing and Engineering; Marcel Dekker, Inc.: New York, NY, USA, 1975; Volume 3, pp. 9–50. ISBN 0-8247-6346-7.
31. Ferro, S.P.; Principe, R.J.; Goldschmit, M.B. A new approach to the analysis of vessel residence time distribution curves. *Metall. Mater. Trans. B* **2001**, *32*, 1185–1193. [CrossRef]
32. Merder, T.; Pieprzyca, J.; Saternus, M. Analysis of residence tome distribution (RTD) curves for T-type tundish equipped in flow control devices—physical modelling. *Metalurgija* **2014**, *53*, 155–158.

33. Kumar, A.; Koria, S.C.; Mazumdar, D. An assessment of fluid flow modeling and residence time distribution phenomena in steelmaking tundish systems. *ISIJ Int.* **2004**, *44*, 1334–1341. [CrossRef]
34. Chattopadhyay, K.; Isac, M.; Gutrie, R.I.L. Modelling of non-isothermal melt flows in a four-strand delta shaped billet caster tundish validated by water model experiments. *ISIJ Int.* **2012**, *52*, 2026–2035. [CrossRef]
35. Ramos-Gomez, E.; Zenit, R.; Gonzalez-Rivera, C.; Trapaga, G.; Ramirez-Argaez, M. Mathematical modelling of fluid flow in a water of an aluminum degassing ladle equipped with impeller-injector. *Metall. Mater. Trans. B* **2013**, *44*, 423–435. [CrossRef]
36. Saternus, M. Influence of impeller shape on the gas bubbles dispersion in aluminum refining process. *J. Achiev. Mater. Manuf. Eng.* **2012**, *55*, 285–290.
37. Chin, E.J.; Celik, C.; Hayes, P.; Bouchard, P.; Larouche, G. GIFS—A novel approach to in-line treatment of aluminum. In *Light Metals, the Minerals, Metals and Materials Society*; TMS: Anaheim, CA, USA, 1994; pp. 929–936.